Sensors and Materials, Vol. 24, No. 1 (2012) 31–41
MYU Tokyo

S & M 0867

Sensing Properties of Impedancemetric Solid-Electrolyte NO_x Sensor Using Perovskite-Type Lanthanum Manganite-Based Receptor

Hong-Chan Cho, Shinya Kuramoto, Satoko Takase,
Jeong-Hwan Song[1] and Youichi Shimizu[*]

Department of Applied Chemistry, Graduate School of Engineering,
Kyushu Institute of Technology, Kitakyushu 804-8550, Japan
[1]Department of Information and Electronic Materials Engineering,
PaiChai University, Daejeon 302-735, Korea

(Received April 7, 2011; accepted June 16, 2011)

Key words: Impedancemetric, NO_x sensor, solid electrolyte, lanthanum manganite

Solid-state impedancemetric NO_x sensor devices composed of the perovskite-type oxide ($La_{0.8}A_{0.2}MnO_3$; A = La, Na, K) as a receptor material and a $Li_{1.5}Al_{0.5}Ti_{1.5}(PO_4)_3$ (LATP) disc as a solid-electrolyte transducer were investigated for the detection of NO_x (NO and NO_2) in the range of 100–500 ppm at 400°C. The lanthanum manganite/LATP-based sensor devices showed NO_x sensing responses that could be divided into two components of resistance and capacitance. While the sensitivities to NO_x were largely affected by the type of receptor material used, the $La_{0.8}K_{0.2}MnO_3$/LATP-based impedancemetric sensor element showed excellent NO sensing properties. FT-IR measurements revealed that the interaction between NO and $La_{0.8}K_{0.2}MnO_3$ was the strongest among the receptor materials.

1. Introduction

Nitrogen oxides (NO_x; NO, NO_2) of exhausts from automobiles and industrial combustible factories are becoming the cause of atmospheric pollutants, such as photochemical smog, acid rain, and so on. Therefore, monitoring the exact amount of nitrogen oxides has become very important for the protection of the global environment in recent years.

[*]Corresponding author: e-mail: shims@che.kyutech.ac.jp

Thus, various types of NO_x gas sensor have been investigated, for example, semiconductor type,[1,2] solid-electrolyte-based potentiometric type,[3–6] amperometric type[6–9] and impedancemetric[10–14] sensors. Among the compact NO_x sensors reported, the solid-electrolyte type is of particular interest from the viewpoints of sensitivity, selectivity, as well as stability at higher temperatures.[15–18] However, these sensor devices still have a rather complicated structure, i.e., they still need reference and/or counter electrodes at the opposite side of the electrolyte.

We have proposed a new type of solid-state simple NO_x sensor combined with a solid-electrolyte as an impedance transducer and an oxide as a receptor.[15–17] The impedancemetric sensor offers an advantage in its single sensor structure, in which there is no need for reference and/or counter electrodes at the opposite side of the sensing electrode. The impedancemetric solid-state sensor using a solid-electrolyte transducer attached with an oxide layer as a gas sensing receptor showed relatively good NO_x sensing properties; however, the impedance changes as the response intensity were as low as several percent for practical applications.[17]

In this study, we have attempted to improve the receptor function using cation-doped lanthanum manganite-based perovskite-type oxide, that is, $La_{0.8}A_{0.2}MnO_3$ (A = La, Na, K) nanopowders prepared by a polymer precursor method. $LaMnO_3$-based oxides have been chosen as the receptor because of its relatively good NO_x sensing properties among the perovskite-type oxides ($LaBO_3$; B = Cr, Mn, Fe, Co, Ni).[17] It was revealed that the use of potassium-doped lanthanum manganite ($La_{0.8}K_{0.2}MnO_3$) as a receptor resulted in about fivefold higher response intensity than that of the nondoped $LaMnO_3$. Here, we report the NO_x sensing performance and the effect of the receptor material on the impedancemetric solid-electrolyte NO_x sensor.

2. Experimental Procedure

2.1 *Synthesis of sensor materials*

Perovskite-type oxide $La_{0.8}A_{0.2}MnO_3$ (A = La, Na, K) nanopowders were prepared by a polymer precursor method.[19–21] Metal (La, Na, K, Mn) nitrates were dissolved in 30 mL of ethylene glycol (EG), which was then mixed with 40 mmol of acetyl acetone (AcAc) and 7 wt% polyvinylpyrolidone (PVP). The solution was treated in an ultrasonic bath for 30 min, then dried at 85°C. The obtained metal-complex precursor was precalcined at 350°C for 7 h, and finally calcined at 650°C for 2 h.

A $Li_{1.5}Al_{0.5}Ti_{1.5}(PO_4)_3$ (LATP) disc was prepared by a sol-gel method.[15–19,22,23] Aqueous solutions of $LiNO_3$, $Al(NO_3)_3 \cdot 9H_2O$, $TiO(CH_2COCH_2COCH_3)_2$ and $(NH_4)H_2PO_4$ were mixed and evaporated at 75°C. The obtained fine xerogel powder was ground and precalcined at 500°C for 3 h. The calcined material was reground and pressed into a sample disc under 520 MPa, and then finally sintered at 1000°C for 6 h. The products were characterized by X-ray diffractometry (XRD) (JDX-3500K, JEOL) using Cu-$K_{\alpha 1}$ radiation and Fourier transform infrared spectroscopy (FT-IR) (IR Prestige-21, SHIMADZU). Specific surface areas of the obtained powders were determined by Brunauer-Emmett-Teller (BET) analysis (Belsorp-mini, BEL) using N_2 adsorbent at 77 K.

2.2 *Fabrication of sensor devices*

The sensor structure consisted of an LATP disc, a perovskite-type oxide layer, and Au electrodes at the opposite surface of the disc as shown in Fig. 1. The Au electrodes were tightly coated with an inorganic adhesive (Aron Ceramic, TOAGOSEI). A paste prepared with receptor powder, turpentine oil, and PVP was painted onto the surface of the LATP disc, and dried and sintered at 500°C for 2 h. NO_x sensing experiments were carried out in a conventional flow apparatus equipped with a heating facility at 300–500°C. Sample gases containing NO or NO_2 were prepared from each parent gas, i.e., NO diluted with nitrogen or NO_2 diluted with a dry synthetic air (N_2 + O_2 gas mixture), by mixing it with N_2 (99.999 vol%) or air at a total flow rate of 100 mL/min. The sensor responses (resistance and capacitance) were measured with an impedance analyzer (LCR 3532-50, HIOKI) between 50 Hz and 5 MHz. The value of the relative sensitivity (S_R or S_C) was defined as $S_R = (R_{gas} - R_{air}) / R_{air} \times 100$ (%) or $S_C = (C_{gas} - C_{air}) / C_{air} \times 100$ (%), in which R_{gas} (C_{gas}) or R_{air} (C_{air}) is resistance (capacitance) in gas or air, respectively.

3. Results and Discussion

3.1 *Preparation of sensing material.*

XRD patterns of the $La_{0.8}A_{0.2}MnO_3$ (A = La, Na, K) perovskite-type oxides prepared by the polymer precursor method are shown in Fig. 2(a). They showed well-crystallized and almost single-phase orthorhombic-type perovskite-type oxides. Figure 2(b) shows

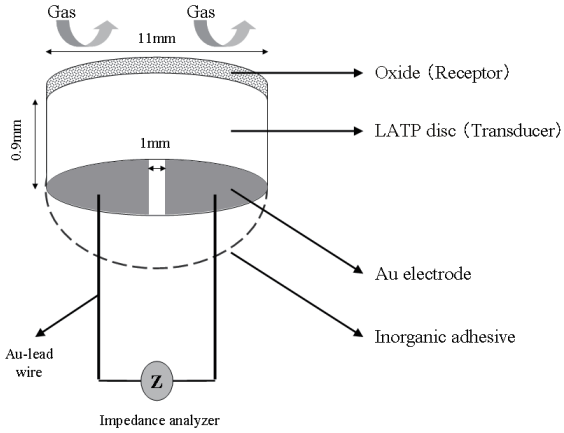

(a)

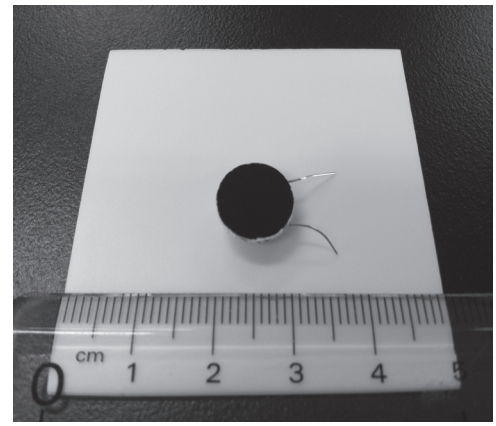

(b)

Fig. 1. Schematic diagram (a) and photograph (b) of the sensor device using perovskite-type oxide (receptor) and LATP (transducer).

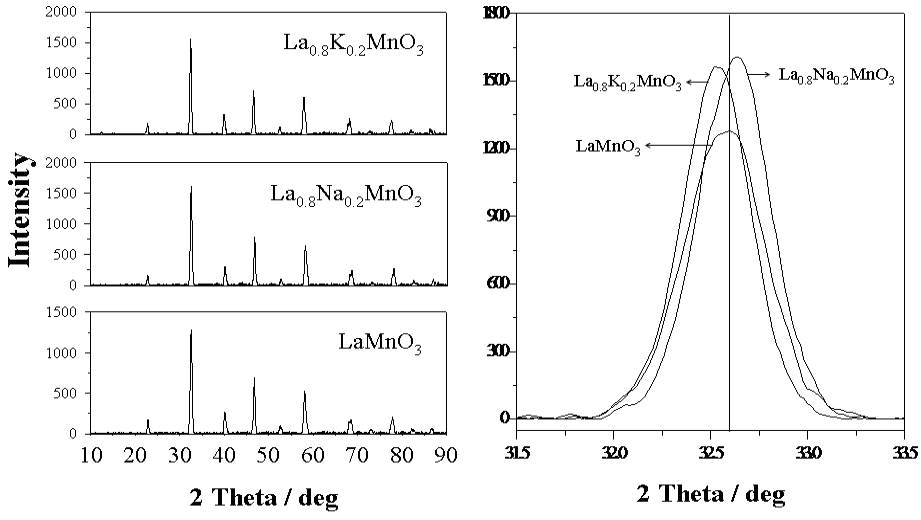

Fig. 2. XRD patterns of $La_{0.8}A_{0.2}MnO_3$ (A = La, Na, K) powders prepared by (a) the polymer precursor method at the wide range between 10 and 90°, and (b) the enlarged portion between 31.5 and 33.5°.

the magnified portion of the XRD patterns between 31.5 and 33.5° of the $La_{0.8}A_{0.2}MnO_3$ (A = La, Na, K) powders. It could be seen that the 2θ values of $La_{0.8}Na_{0.2}MnO_3$ and $La_{0.8}K_{0.2}MnO_3$ at approximately 32.5° were increased and decreased compared with that of $LaMnO_3$, respectively, which showed the change in lattice constant. Table 1 summarizes the lattice parameters and BET surface areas of these $La_{0.8}A_{0.2}MnO_3$ (A = La, Na, K) oxides. The distance at the (111) plane (d_{111}) of $La_{0.8}Na_{0.2}MnO_3$ and $La_{0.8}K_{0.2}MnO_3$ decreased and increased, respectively, compared with that of $LaMnO_3$, which corresponds to an increase and a decrease in the value of 2θ angles. The lattice volume of $La_{0.8}Na_{0.2}MnO_3$ was smaller than that of $LaMnO_3$, which indicates that the cation exchange in the crystal was caused by the difference in the ion radii of Na^+ (0.97 Å) and La^{3+} (1.14 Å). On the other hand, the lattice parameter of b in $La_{0.8}K_{0.2}MnO_3$ was expanded by introducing K^+ (1.33 Å) ion, which has a larger ion radius than La^{3+} (1.14 Å). On the other hand, the lattice parameters of a and c in $La_{0.8}K_{0.2}MnO_3$ were shrunk and the lattice volume of $La_{0.8}K_{0.2}MnO_3$ was not changed much from that of $LaMnO_3$. It was also found that the orthorhombic distortion of $LaMnO_3$ was eased to the cubic phase by K^+ doping in $LaMnO_3$, as shown in Table 1. The specific surface areas of the $La_{0.8}A_{0.2}MnO_3$ (A = La, Na, K) oxides prepared by the polymer precursor method were 16.2, 14.1, and 10.8 m^2/g, respectively, as also shown in Table 1.

Table 1
Lattice parameters and specific surface areas of $La_{0.8}A_{0.2}MnO_3$ (A = La, Na, K).

Oxide	Lattice parameter			Lattice volume ($Å^3$)	Distance at (111) plane (d_{111}) (Å)	BET surface area (m^2/g)
	a (Å)	b (Å)	c (Å)			
$LaMnO_3$	3.8846	3.8545	3.9198	58.69	2.7444	16.2
$La_{0.8}Na_{0.2}MnO_3$	3.8831	3.8530	3.9138	58.56	2.7411	14.1
$La_{0.8}K_{0.2}MnO_3$	3.8807	3.8795	3.8960	58.65	2.7493	10.8

3.2 *Sensing behavior of impedance-metric NO_x sensors*

The NO and NO_2 response properties of the impedancemetric sensor using nondoped $LaMnO_3$ receptor and LATP transducer were firstly examined. Figure 3 shows Nyquist's plots of the $LaMnO_3$/LATP sensor at a frequency range from 50 Hz to 5 MHz in air, 100 ppm NO, and 100 ppm NO_2 at 400°C. This sensor showed the impedance change by changing the NO gas from air to NO (or NO_2) especially at the lower frequency region of the interface impedance area. However, the noise in the sensor response was increased at lower frequency area, so we investigated the response characteristic of the sensor at the fixed frequency of 100 Hz as a sensing signal. The impedance response of the $LaMnO^3$/LATP sensor could be divided into two components: resistance (R) and capacitance (C). Figure 4 shows the response curves of each resistance component (R) and capacitance component (C) of the $LaMnO_3$/LATP sensor for various concentrations of NO at 400°C, 100 Hz. The $LaMnO_3$/LATP sensor showed good response for each NO concentration. The sensing properties of each resistance (S_R) and capacitance (S_C) of the $LaMnO_3$/LATP sensor at 400°C are shown in Fig. 5. A good sensing property was found to be comparatively obtained as both resistance component (R) and capacitance component (C); the resistance component was obtained as a negative response and the capacitance component was obtained as a positive response for the $LaMnO_3$/LATP sensor.

In the same way, for the other $La_{0.8}A_{0.2}MnO_3$ (A = Na, K) systems, perovskite-type oxide receptors were examined. The sensing properties of each resistance (S_R) and capacitance (S_C) of the $La_{0.8}A_{0.2}MnO_3$/LATP sensor for various concentrations of NO are shown in Fig. 6. The response property of excellent resistance or capacitance change was observed in the case of NO at 400°C for the $La_{0.8}K_{0.2}MnO_3$/LATP sensor. For the resistance component (R) of the sensor responses, those of the $La_{0.8}Na_{0.2}MnO_3$/LATP and $La_{0.8}K_{0.2}MnO_3$/LATP sensors increased with increasing NO concentration. On the other hand, for the capacitance component (C) of those sensor devices, the capacitance of the $La_{0.8}K_{0.2}MnO_3$/LATP sensor decreased with increasing NO concentration, whereas the capacitance of the $La_{0.8}Na_{0.2}MnO_3$/LATP sensor increased with increasing NO concentration.

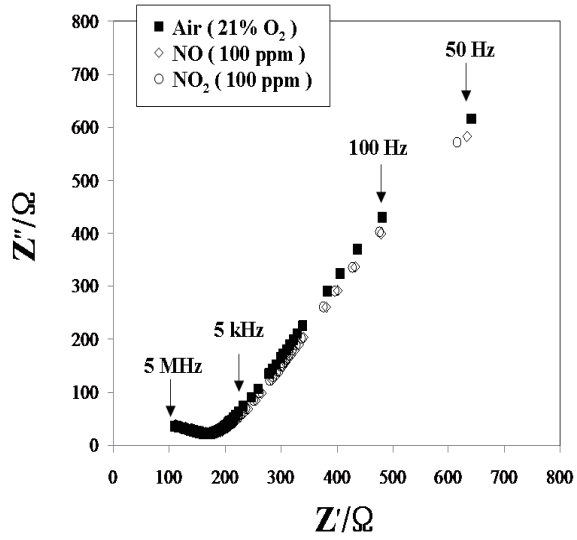

Fig. 3. Nyquist's plots of the $LaMnO_3$/LATP sensor at frequency range from 50 Hz to 5 MHz in air, 100 ppm NO, and 100 ppm NO_2 at 400°C.

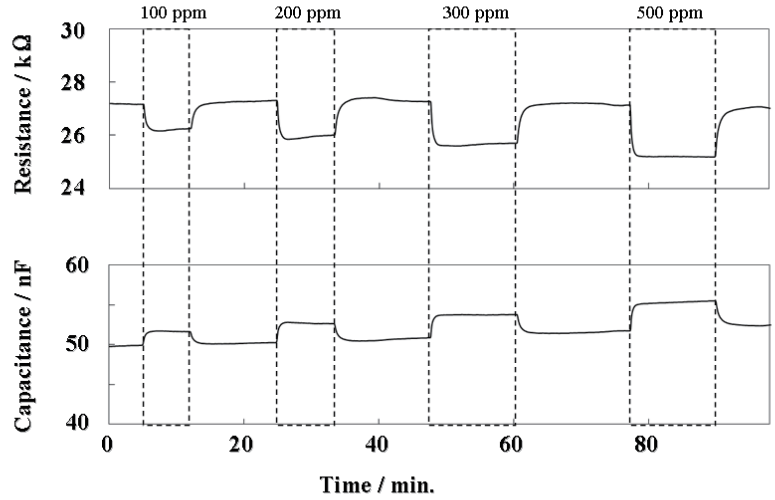

Fig. 4. Response transient curves of the $LaMnO_3$/LATP sensor for various concentrations of NO at 400°C, 100 Hz.

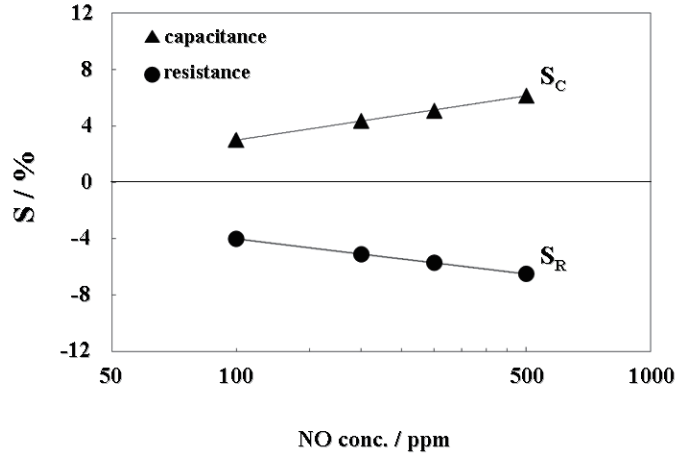

Fig. 5. Sensing properties of the $LaMnO_3$/LATP sensor for various concentrations of NO at 400°C, 100 Hz.

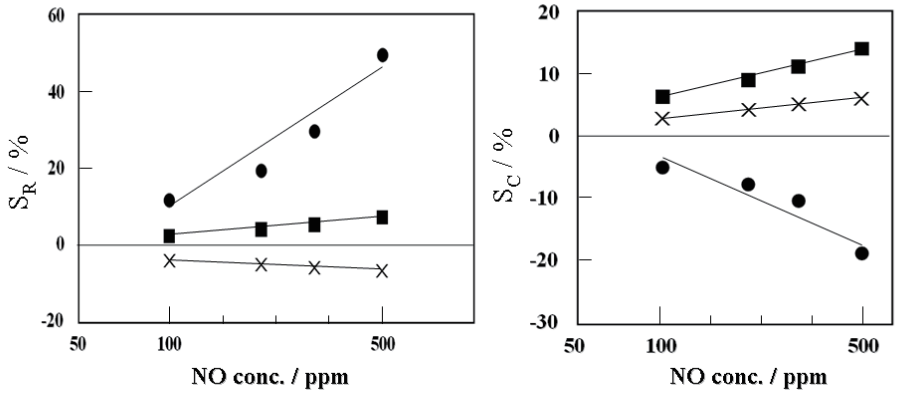

Fig. 6 Sensing properties of the $La_{0.8}A_{0.2}MnO_3$ (A = La, Na, K)/LATP sensors for various concentrations of NO at 400°C, 100 Hz. (× $LaMnO_3$, ■ $La_{0.8}Na_{0.2}MnO_3$, ● $La_{0.8}K_{0.2}MnO_3$).

The response sensitivities of resistance (S_R) and capacitance (S_C) of various sensor elements for both NO and NO_2 are summarized in Fig. 7. The $La_{0.8}A_{0.2}MnO_3$ (A = Na, K)/LATP sensors showed higher response sensitivity to both NO and NO_2 at 400°C than that of using $LaMnO_3$ oxide, in spite of the low specific surface areas of $La_{0.8}A_{0.2}MnO_3$ (A = Na, K) oxides. Figure 8 shows response sensitivities of the $La_{0.8}K_{0.2}MnO_3$/LATP

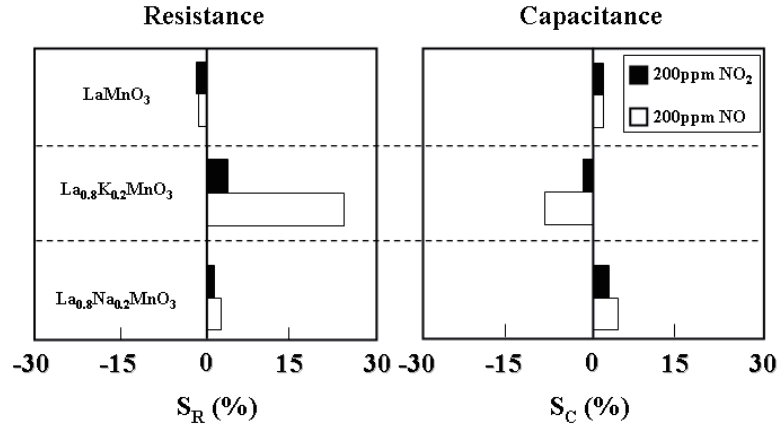

Fig. 7. Response sensitivities of the $La_{0.8}A_{0.2}MnO_3$ (A = La, Na, K)/LATP sensors for NO and NO_2 at 400°C, 100 Hz.

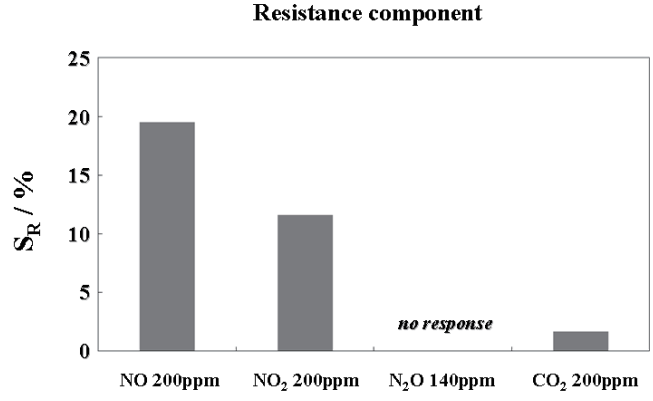

Fig. 8. Response sensitivities of the $La_{0.8}K_{0.2}MnO_3$/LATP sensor to NO, NO_2, N_2O, and CO_2 at 400°C, 100 Hz.

sensor to NO, NO_2, N_2O, and CO_2 at 400°C, 100 Hz. The $La_{0.8}K_{0.2}MnO_3$/LATP sensor showed the highest sensitivity of the resistance component among all the sensors examined for NO, although no remarkable difference in capacitance of the sensors was observed. Furthermore, the sensor showed no response or a small response to N_2O and CO_2, respectively.

A large difference was found in the sensor responses to NO at 400°C, as stated above. NO absorption properties on $La_{0.8}A_{0.2}MnO_3$ (A = La, Na, K) surfaces were characterized by FT-IR spectrometry. Figure 9 shows FT-IR spectra of the oxides before and after treatment with 100 ppm NO at 400°C for 30 min. The starting adsorption peaks at around 600 cm^{-1} of all the oxides could be assigned as ν (Mn-O) in the perovskite-type oxides. After the NO treatment, adsorption peaks at 1385 cm^{-1}, which could be assigned as ν (NO_3^-), were observed. Adsorption peaks of NO_3^- could be produced by the reaction between NO and adsorbed oxygen. The strongest ν (NO_3^-) peak at 1385 cm^{-1} was detected on $La_{0.8}K_{0.2}MnO_3$.[24–26] This should be one of the reasons for the high NO sensitivity of the $La_{0.8}K_{0.2}MnO_3$/LATP sensor. Adsorption peaks at 1600 and 2400 cm^{-1} could be noticed in the region of ν (C=O) and ν (CO^2), which could come from atmospheric carbon dioxide.[26,27] However, the sensing mechanism of the present electrochemical device still needs further investigation.

The sensor mechanism of this new type of solid-electrolyte impedancemetric is shown in Fig. 10. As the p-type oxides were used as the receptor, electrons trapped by adsorbed oxygen were flowed into the receptor when the adsorbed oxygen was consumed with NO or NO_2. Consequently, the amount of carrier holes in the receptor was decreased. Then, Li^+ in the solid electrolyte moved more freely because of the electrical force from the holes in the receptor. The resistance of the solid electrolyte

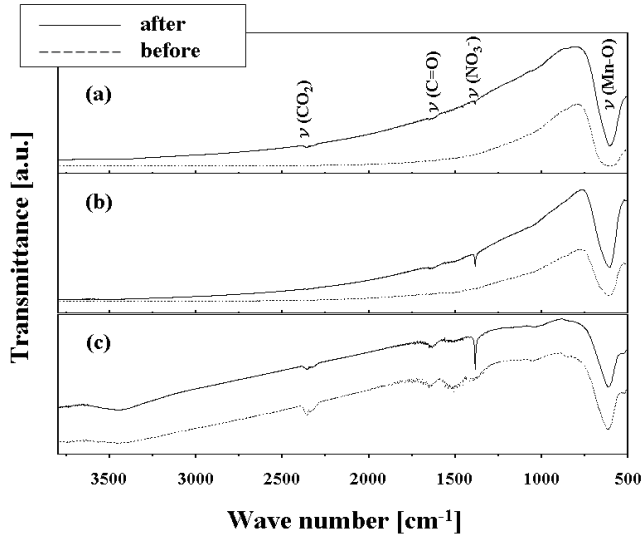

Fig. 9. FT-IR spectra of (a) $LaMnO_3$, (b) $La_{0.8}Na_{0.2}MnO_3$, and (c) $La_{0.8}K_{0.2}MnO_3$ powders before and after treatment with 100 ppm NO at 400°C for 30 min.

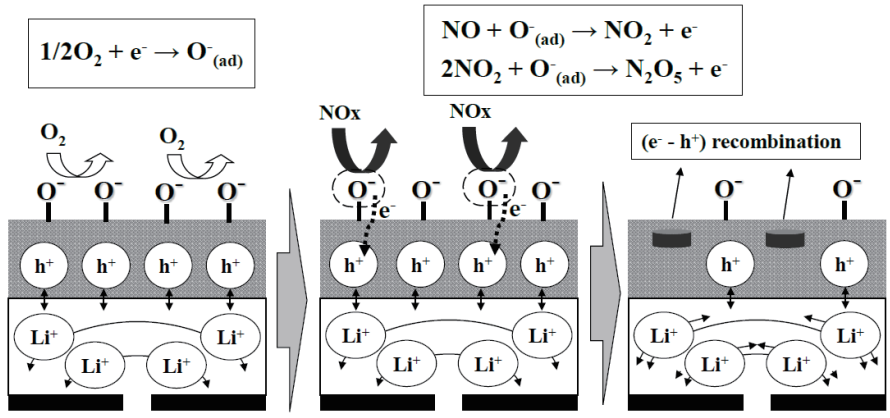

Fig. 10. Response mechanism of the oxide/LATP sensor.

should be increased by the expansion of the distance of mobile Li^+, and the capacitance of the solid electrolyte was also increased with increasing amount of mobile Li^+. As the interface between the receptor and transducer seems to play an important role in the sensing mechanism, the design of the optimum sensor structure in the receptor and transducer layers should improve the sensor performance. Further investigations on the sensing mechanism and sensor structure are now in progress.

4. Conclusions

An impedancemetric sensor has been designed using perovskite-type ($La_{0.8}A_{0.2}MnO_3$; A = La, Na, K) oxide receptors and Li^+-ionic conductor ($Li_{1.5}Al_{0.5}Ti_{1.5}(PO_4)_3$; LATP) transducer. The impedance responses of the NO_x sensors could be obtained as components of resistance and capacitance. Moreover, they showed dependence on each NO_x concentration and selectivity of NO and NO_2. The sensitivities of these sensors were affected by the ability of receptor materials to detect the gas at different NO_x concentrations and the $La_{0.8}K_{0.2}MnO_3$ receptor gave the highest sensitivity among the sensors.

Acknowledgements

The authors are grateful to the Center for Instrumental Analysis, Kyushu Institute of Technology for XRD measurement. This work was partially supported by the NISSAN Science Foundation, Japan and by the International Cooperative Subject for Industrial-Academic Common Technology Development (200800030050) of SMBA for Collaboration R&D between Industry and Academy, Korea.

References

1 M. Akiyama, J. Tamaki, N. Miura and N. Yamazoe: Chem. Lett. **20** (1991) 1611.
2 M. Akiyama, Z. Zhang, J. Tamaki, N. Miura, N. Yamazoe and T. Harada: Sens. Actuators, B **13/14** (1993) 619.
3 A. Huerland, R. Moos, R. Mueller, C. Plog and U. Simon: Sens. Actuators, B **77** (2001) 287.
4 P. Elumalai, V. V. Plashnitsa, Y. Fujio and N. Miura: Sens. Actuators, B **144** (2010) 215.
5 J. S. Park, B. Y. Yoon, C. O. Park and W. J. Lee: Sens. Actuators, B **135** (2009) 516.
6 N. Miura, G. Lu and N. Yamazoe: Sens. Actuators, B **52** (1998) 169.
7 N. Miura, M. Iio, G. Lu and N. Yamazoe: Sens. Actuators, B **35/36** (1996) 124.
8 A. Dutta and T. Ishihara: Sens. Actuators, B **108** (2005) 309.
9 M. Ono, K. Shimanoe, N. Miura and N. Yamazoe: Solid State Ionics **136/137** (2000) 583.
10 N. Miura, M. Nakatou and S. Zhuiykov: Sens. Actuators, B **93** (2003) 221.
11 R. Wama, M. Utiyama, V. V. Plashnitsa and N. Miura: Electrochem. Commun. **9** (2007) 2774.
12 L. Y. Woo, R. S. Glass, R. F. Novak and J. H. Visser: J. Electrochem. Soc. **157** (2010) 81.
13 K. Shimizu, K. Kashiwagi, H. Nishiyama, S. Kakimoto, S. Sugaya, H. Yokoi and A. Satsuma: Sens. Actuators, B **130** (2008) 707.
14 L. Y. Woo, L. P. Martin and R. S. Glass: J. Electrochem. Soc. **155** (2008) 32.
15 D. Koba, S. Takase and Y. Shimizu: ECS Trans. **3** (2006) 163.
16 Y. Shimizu, D. Koba, H. Saitoh and S. Takase: ECS Trans. **1** (2006) 131.
17 Y. Shimizu, S. Takase and D. Koba: Adv. Mater. Res. **47–50** (2008) 479.
18 S. Tamura, I. Hasegawa and N. Imanaka: Sens. Actuators, B **130** (2008) 46.
19 Y. Shimizu and T. Murata: J. Am. Ceram. Soc. **80** (1997) 2702.
20 Y. Shimizu, S. Takase and M. Yoshida: Adv. Sci. Technol. **45** (2006) 1792.
21 M. Popa, J. Frantti and M. Kakihana: Solid State Ionics **154/155** (2002) 135.
22 K. Oda, S. Takase and Y. Shimizu: Mater. Sci. Forum **544/545** (2007) 1033.
23 A. S. Besta, M. Forsyth and D. R. MacFarlane: Solid State Ionics **136/137** (2000) 339.
24 S. J. Huang, A. B. Walters and M. A. Vannice: J. Catal. **192** (2000) 29.
25 T. M. Salama, M. M. Mohamed, I. Othman and G. A. El-Shobaky: Appl. Catal., A **286** (2005) 85.
26 L. Liu, B. Liu, L. Dong, J. Zhu, H. Wan, K. Sun, B. Zhao, H. Zhu, L. Dong and Y. Chen: Appl. Catal., B **90** (2009) 578.
27 F. Gasc, S. Thiebaud-Roux and Z. Mouloungui: J. Supercrit. Fluids **50** (2009) 46.